Analysis of Limit Cycle in Control Systems for Joint-Dominated Structures

Mathieu Mercadal* and Wallace E. Vander Velde†
Massachusetts Institute of Technology, Cambridge, Massachusetts

The use of joints with large tolerances is necessary in the deployment process of large space truss structures. They, unfortunately, introduce nonlinearities in the structure and can generate phenomena such as limit cycles when active control feedback is applied. Predicting limit cycles and their stability can be done analytically for large, controlled, joint-dominated structures. The procedure involves first approximating the joints as linear elements and performing a standard modal decomposition of the linearized system. This analysis is performed only once and provides a reduced-order linear model that can be modified by the introduction of various control laws. The nonlinear parts of the joints' behavior are then fed back to the linear model. When the signals are approximated to the first harmonic only, the use of describing functions allows the derivation of nonlinear algebraic equations that must be satisfied by the dynamical parameters when a limit cycle exists. Stability conditions are found by perturbing the approximate limit cycle only along the state-space plane it occupies.

I. Introduction

DEPLOYABLE or erectable truss structures, such as the COFS I experimental mast envisioned by NASA, share the characteristic of being assembled by means of joints having rather large tolerances. There will be some appreciable differences between the dynamics of such structures and the dynamics of similar continuous trusses. Constraints in the construction process, however, dictate such a choice.

The use of joints with large tolerances is likely to increase the flexibility of the structures. The resulting alteration of the structural dynamics due to the flexibility can range from a mere shift in modal frequencies to complete changes in modal frequencies and mode shapes. The joint dynamics might even account preponderantly for the response of the entire structure.

Some nonlinear effects are also likely to appear, due, for example, to play in the joints or Coulomb friction. The presence of the joints therefore gives birth to a whole new variety of dynamical problems, particularly if active control has to be applied to the structures.

The use of an active control system is required to suppress the vibrations that occur in large flexible structures. The design of a controller is greatly simplified if the system to control is a linear time invariant (LTI) system. The problem of designing a controller for a structure with rigid joints or for a structure with nonrigid joints can be treated the same way, provided the displacement in the structure is kept small and provided the nonrigid joints behave linearly. Unfortunately, the same approach cannot be used if the nonlinear behavior of the joints cannot be neglected, which is the case if the structure's dynamics are joint dominated. The structure must then be studied as a nonlinear system.

Among the new problems raised by the existence of nonlinearities, one of foreseen importance is the possible occurrence of limit cycles in the control system that might result from the lags generated by the nonlinear joints. A limit cycle is a sustained oscillation of a dynamical system, and it has, therefore, the same potentially damaging effects on the completion of a mission as free oscillations when the system is a structure.

Received Aug. 20, 1987; revision received Jan. 15, 1988.

*Research Assistant, Ph.D. Candidate.
†Professor of Aeronautics and Astronautics. Fellow AIAA.

The purpose of this paper is to present an analytical tool that allows the prediction of limit cycles and the determination of their stability in large, flexible, joint-dominated structures under active control similar to the COFS mast.

II. Modeling of the Problem

Methods to analyze limit cycles in dynamical systems in the form of a linear plant with a nonlinear feedback (Fig. 1) have been derived and successfully used, mostly in single-input/single-output (SISO) cases. Many books have appeared on the subject of oscillations in nonlinear systems; among them are Refs. 1–3. Generalization to the multi-input/multi-output (MIMO) case has also been presented in Ref. 4.

It is possible to model a truss structure as a nonlinear feedback dynamical system. Some restricting hypotheses have, however, to be made about the joints dynamics, but those are expected to hold in most cases. What will be assumed hereafter is that there exists a *linear* load-displacement law $\boldsymbol{F}^l(\epsilon)$ such that

$$\|\boldsymbol{F}(\epsilon) - \boldsymbol{F}^l(\epsilon)\| / \|\epsilon\| \to 0 \text{ as } \epsilon \to \infty \tag{1}$$

where $\boldsymbol{F}(\epsilon)$ represents the *actual* load-displacement law. This rules out nonlinearities such as spring hardening, or spring softening. The hypothesis holds, however, for strong nonlinearities at the origin such as the one observed in the load-displacement law of a pinned joint presented in Fig. 2. For such a joint, the nonlinearity is mostly due to play around the pin, and as the displacement increases, the joints behave more and more like linear elements until the limit of elasticity of their constituting material is reached.

III. Mathematical Formulation

In the following, D represents the domain occupied by the point P of the structure; S denotes a surface where boundary conditions are applied; $\boldsymbol{u}(P,t)$ is the displacement at time t of the point P. The structure is supposed to have N joints, each of which is identified by an index $j = 1,2,\ldots, N$. For joint j, P_{j1} and P_{j2} denote the two endpoints by which the joint is connected to the rest of the structure. The efforts applied by the joints on the rest of the system will be concentrated at those endpoints only. The efforts transmitted by a joint j are supposed to depend on the deformation ϵ_j of the joint. In the following, the joints are assumed to be massless.

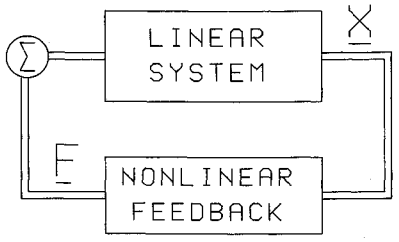

Fig. 1 Linear system with nonlinear feedback.

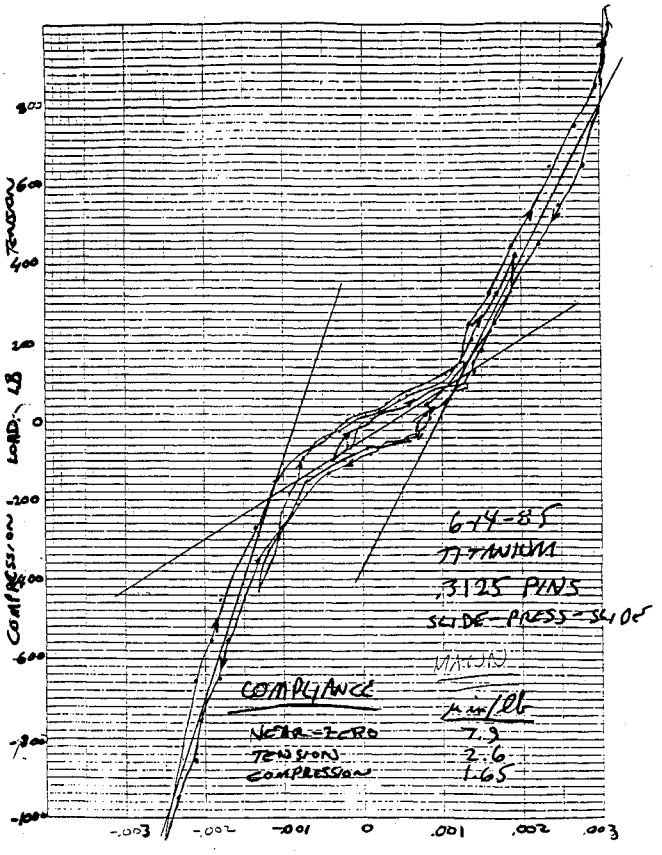

Fig. 2 Typical tension compression data for a pinned joint.

The first step in deriving a nonlinear feedback system model for the structure is to replace the joints by their linear asymptotes. If $F_{jk}(\epsilon)$ is the force applied by the joint j at its end P_{jk}, the force assumed in the linear model is only $F^l_{jk}(\epsilon_j)$ where F^l_{jk} satisfies Eq. (1). The resulting structure is linear under the usual assumption of small displacements. The equations of the dynamics for such linear structures have the following generic form:

$$Lu + M\ddot{u} = f, \qquad P \in D \tag{2}$$

where L is a differential operator, M a mass matrix, and where $\ddot{u}$ is the second derivative of u with respect to time. It is supposed that the system has no structural damping to simplify the formulation of the equation. The displacement u is also subject to the boundary conditions

$$B_i u = 0, \qquad P \in S, \qquad i = 1,2,...,p \tag{3}$$

where B_i are differential operators; $f(P,t)$ represents the external forcing terms on the linear structure.

Let us define $F^{nl}_{jk}(\epsilon_j)$ as

$$F^{nl}_{jk}(\epsilon_j) \triangleq F_{jk}(\epsilon_j) - F^l_{jk}(\epsilon_j), \qquad k = 1,2, \qquad j = 1,...,N \tag{4}$$

This represents the difference between joint j's real transmitted effort at the end P_{jk} and the linear model of the same quantity that is assumed in the linearized model.

Let us also define an augmented forcing term for the linear structure $f(P,t)$ as

$$f(P,t) \triangleq f_{\text{ext}}(P,t) + \sum_{j=1}^{N} [F^{nl}_{j1}(\epsilon_j)\delta(P - P_{j1}) + F^{nl}_{j2}(\epsilon_j)\delta(P - P_{j2})] \tag{5}$$

where f_{ext} represents the external forcing terms that apply on the real structure, and where $\delta(P)$ is also the spatial Delta function. Equation (2) represents the structure's exact dynamics if the augmented forcing term is used in its right-hand side, since the part of the response of the joints that was neglected to obtain the linear model is reintroduced through $f(P,t)$. This form of modeling is similar to that of Ref. 5. In this case, however, there is no assumption that the nonlinear effects are small.

A modal decomposition of the equivalent linear structure can be performed to transform the *partial differential equation* problem [Eq. (2)] into an infinite system of *ordinary differential equations*. Details about this procedure can be found, for example, in Refs. 5 and 6.

Exact solutions for the modes can seldom be found using Eq. (2). Closed-form solutions only exist for very particular problems. Approximate numerical solutions can, however, be found by discretizing the problem. This procedure, also referred to as a Ritz procedure, consists of considering solutions of Eq. (2) in a finite-dimensional functional space only. In the finite-element method, for example, which is the most straightforward approach, the state of displacement anywhere inside one element is uniquely defined in terms of the nodal displacements that are, in fact, the coefficients of the linear combination of the basic functions that have been retained to approximate the elementary deformations.

Let us call ω_r and $\phi_r(P)$ the modal frequencies and the mode shapes of the discretized structure. Then, the general solution of Eq. (2) will be expanded as

$$u(P,t) \triangleq \sum_{r=1}^{n} q_r(t)\phi_r(P) \tag{6}$$

where n is the number of retained modes. The modal coordinates $q_r(t)$ are scalar functions of time and can be collected into a vector $q \triangleq [q_1,q_2,...,q_n]^T$. When plugging Eq. (6) into Eq. (2), the dynamical equations become the following system of differential equations:

$$\ddot{q} + \Lambda q = F \tag{7}$$

where $F \triangleq [f_1,f_2,...,f_n]^T$ and $\Lambda \triangleq \text{diag}(\omega_1^2,\omega_2^2,...,\omega_n^2)$.

As the discretization is refined or, equivalently, as the dimension of the solution subspace is increased, a solution of Eq. (7) will tend to its limit, which is the exact solution of Eq. (2). It is therefore possible to control the precision of the solution.

It is crucial that the finite-dimensional solution subspace be as close as possible to the infinite-dimensional solution space so that the approximate solution retains most of the exact solution. In this context, the importance of the hypothesis [Eq. (1)] made about the joints' behavior becomes clear: were all the modes to be used, it would not matter what orthonormal basis is chosen on which to expand the solution. Conversely, if the solution is expanded on a finite-dimensional space only, the modes chosen must retain the principal features of the behavior of the real system. The asymptotic linearity of the joints guarantees that the equivalent linear model that generates the solution subspace yields a meaningful description of the dynamics of the structure.

The forcing term F can be further developed to separate the real external forcing terms from the extra terms that were intro-

duced to obtain the augmented excitation. $\boldsymbol{F}$ can be written as

$$\boldsymbol{F} = B_j \boldsymbol{F}_j + B_c \boldsymbol{F}_c + B_d \boldsymbol{d} \tag{8}$$

where $\boldsymbol{F}_j$ is a vector formed by the nonlinear remaining parts of the efforts applied at one end of the joints

$$\boldsymbol{F}_j \triangleq [\boldsymbol{F}_{j1}^{nlT}(\epsilon_1), \ldots, \boldsymbol{F}_{N1}^{nlT}(\epsilon_N)]^T \tag{9}$$

and where B_j is the following matrix:

$$B_j = \begin{vmatrix} \boldsymbol{\phi}_1^T(P_{l1}) - \boldsymbol{\phi}_1^T(P_{12}) & \cdots & \boldsymbol{\phi}_1^T(P_{N1}) - \boldsymbol{\phi}_1^T(P_{N2}) \\ \boldsymbol{\phi}_2^T(P_{l1}) - \boldsymbol{\phi}_2^T(P_{12}) & \cdots & \boldsymbol{\phi}_2^T(P_{N1}) - \boldsymbol{\phi}_2^T(P_{N2}) \\ \vdots & & \vdots \\ \boldsymbol{\phi}_n^T(P_{l1}) - \boldsymbol{\phi}_n^T(P_{12}) & \cdots & \boldsymbol{\phi}_n^T(P_{N1}) - \boldsymbol{\phi}_n^T(P_{N2}) \end{vmatrix} \tag{10}$$

$\boldsymbol{F}_c$ corresponds to the controls applied on the system, and $\boldsymbol{d}$ denotes possible disturbances. If the controls are discrete and applied at some points P_{c1} to P_{cm}, the structure of the B_c matrix will be

$$B_c = \begin{vmatrix} \boldsymbol{\phi}_1^T(P_{c1}) & \boldsymbol{\phi}_1^T(P_{c2}) & \cdots & \boldsymbol{\phi}_1^T(P_{cm}) \\ \boldsymbol{\phi}_2^T(P_{c1}) & \boldsymbol{\phi}_2^T(P_{c2}) & \cdots & \boldsymbol{\phi}_2^T(P_{cm}) \\ \vdots & \vdots & & \vdots \\ \boldsymbol{\phi}_n^T(P_{c1}) & \boldsymbol{\phi}_n^T(P_{c2}) & \cdots & \boldsymbol{\phi}_n^T(P_{cm}) \end{vmatrix} \tag{11}$$

where

$$\boldsymbol{F}_c \triangleq [\boldsymbol{F}_{c1}^T(t), \boldsymbol{F}_{c2}^T(t), \ldots, \boldsymbol{F}_{cm}^T(t)]^T \tag{12}$$

If a linear feedback control law of the form

$$\boldsymbol{F}_c = -G_1 \boldsymbol{q} - G_2 \dot{\boldsymbol{q}} \tag{13}$$

were to be used, Eq. (7) could be written as

$$\ddot{\boldsymbol{q}} + B_c G_2 \dot{\boldsymbol{q}} + (\Lambda + B_c G_1)\boldsymbol{q} = B_j \boldsymbol{F}_j(\boldsymbol{q}, \dot{\boldsymbol{q}}) \tag{14}$$

The left-hand side of the equation represents an LTI system, whereas the right-hand side constitutes a nonlinear feedback.

The form of Eq. (13) was indicated for the control law because it is a very commonly used class of controller. However, the modeling can clearly accommodate any type of controller, even nonlinear. The important point is that the separation of the joint load-displacement characteristics into a linear part, which dominates at large displacements, and a nonlinear part, permits the definition of a linear model for the structure with a standard modal analysis. This analysis can be performed using the finite-element method, for example. This expensive analysis is performed only once. The dynamical model it yields is corrected by feeding back the residual nonlinear effects of the joints as well as the control law, which can be of any type. The effect of the nonlinear part of the joint characteristics can thus be studied in the context of a reduced modal model of the linear part of the system dynamics, rather than incorporating a nonlinear description of the joints directly in the finite-element model of the structure, which is of very high order.

IV. Limit Cycle Analysis

It is assumed here that the nonlinearities in the joints can be separated into SISO nonlinear effects. For every joint j, the nonlinear term F_{j1}^{nl} can be written as the sum

$$\boldsymbol{F}_{j1}^{nl}(\boldsymbol{q}, \dot{\boldsymbol{q}}) = \boldsymbol{z}^{j1} n^{j1}(x_1, \dot{x}_1) + \boldsymbol{z}^{j2} n^{j2}(x_2, \dot{x}_2) + \cdots + \boldsymbol{z}^{jp} n^{jp}(x_p, \dot{x}_p) \tag{15}$$

where $\boldsymbol{z}^{jk}$ are fixed direction vectors, n^{jk} are scalar nonlinear functions, and x_k are scalar quantities that depend on the state variables. It is assumed here that more than one single nonlinearity can be present in a joint, but that these nonlinearities have SISO character. A first nonlinearity could be, for example, the axial load. The axial load, occurring principally in a single direction z^1 along the joint's axis, depends mostly on the axial deformation of the joint, which can be the variable x_1 in that case. At the same time, the axial torsion could also be nonlinear. The torsional torque appears principally in the direction z^2 along the joint's axis, and it depends mostly on the torsion, which would then be the parameter x_2. Assuming no coupling between the two effects just described, these can be treated independently.

A second assumption is that the linear part of the system filters out the input signals it receives so that only the first harmonic subsists. Such an assumption seems reasonable when the linear plant includes the feedback law: the resonant peaks that appear at high frequencies in the free structure must indeed be attenuated by the controls in that case—at least in some frequency band near the controlled frequencies.

Under the two previous assumptions, dual input describing functions (DIDF) can be used to model the nonlinearities in the system. DIDF apply in a SISO context. If the input x of a generic nonlinear function y is the sum of a bias and a sine wave as

$$x = B + A \exp(j\omega t), \qquad A, B \in \mathbb{R}$$

the output will be approximated as

$$y = n_B(A,B,\omega)B + n_A(A,B,\omega)A \exp(j\omega t), \qquad n_B \in \mathbb{R}, \qquad n_A \in \mathbb{C}$$

where the gains n_A and n_B are chosen to minimize the integral square error between the real and the approximate signal.[7] They can be computed numerically using experimental data, or in closed form if a mathematical model of the nonlinearity is available.

Let us write the state vector as the sum of a bias and a sine wave

$$\boldsymbol{q} = \boldsymbol{q}^0 + \boldsymbol{q}^1 \exp(j\omega t) \tag{16}$$

where $\boldsymbol{q}^0$ is an n-dimensional real vector and $\boldsymbol{q}^1$ is an n-dimensional complex vector that includes the amplitude as well as the phases of n-sinusoidal signals that have to be considered.

The forcing term $\boldsymbol{F}_j$ can then be approximated as

$$\boldsymbol{F}_j = \mathcal{N}^0(\boldsymbol{q}^0, \boldsymbol{q}^1, \omega)\boldsymbol{q}^0 + \mathcal{N}^1(\boldsymbol{q}^0, \boldsymbol{q}^1, \omega)\boldsymbol{q}^1 \exp(j\omega t) \tag{17}$$

where $\mathcal{N}^0$ and $\mathcal{N}^1$ are two gain matrix functions. It is supposed here that there are more nonlinearities than there are modes retained to describe the system. The variables $\boldsymbol{q}$ are, therefore, preferred to other sets of variables such as the joints displacements or the nonlinear force vector $\boldsymbol{F}_j$. The matrices $\mathcal{N}^0$ and $\mathcal{N}^1$ can be computed using the describing functions of the individual elements as follows. The input to the identified kth nonlinearity in joint j is a linear combination of the state variables:

$$x_k^j = \boldsymbol{C}^{jk}\boldsymbol{q} = \boldsymbol{C}^{jk}\boldsymbol{q}^0 + \boldsymbol{C}^{jk}\boldsymbol{q}^1 \exp(j\omega t) \tag{18}$$

where $\boldsymbol{C}^{jk}$ is a row vector.

Using describing functions, the nonlinear function n^{jk} can be approximated as

$$n^{jk} = n_B^{jk}(|\boldsymbol{C}^{jk}\boldsymbol{q}^1|, \boldsymbol{C}^{jk}\boldsymbol{q}^0, \omega)\boldsymbol{C}^{jk}\boldsymbol{q}^0 + n_A^{jk}(|\boldsymbol{C}^{jk}\boldsymbol{q}^1|, \boldsymbol{C}^{jk}\boldsymbol{q}^0, \omega)\boldsymbol{C}^{jk}\boldsymbol{q}^1 \exp(j\omega t) \tag{19}$$

recognizing that $B_k = \boldsymbol{C}^{jk}\boldsymbol{q}^0$ is a scalar bias and $A_k = |\boldsymbol{C}^{jk}\boldsymbol{q}^1|$ is the scalar amplitude of the sinusoidal signal. The DIDF approximates a scalar quantity that represents the magnitude of one nonlinearity. The resulting forces are just obtained by multiplying the vectors $\boldsymbol{z}^{jk}$, which represent the directions of the

nonlinear efforts by their computed magnitudes. Summing over all the identified nonlinearities for joint j, the forcing F_{j1}^{nl} can be written as

$$F_{j1}^{nl} = \mathcal{N}_j^0(q^0,q^1,\omega)q^0 + \mathcal{N}_j^1(q^0,q^1,\omega)q^1 \exp(j\omega t) \tag{20}$$

where

$$\mathcal{N}_j^0(q^0,q^1,\omega) = \sum_{k=1}^{p} z^{jk} n_B^{jk}(|C^{jk}q^1|, C^{jk}q^0, \omega)C^{jk} \tag{21a}$$

and

$$\mathcal{N}_j^1(q^0,q^1,\omega) = \sum_{k=1}^{p} z^{jk} n_A^{jk}(|C^{jk}q^1|, C^{jk}q^0, \omega)C^{jk} \tag{21b}$$

The matrices $\mathcal{N}^0(q^0,q^1,\omega)$ and $\mathcal{N}^1(q^0,q^1,\omega)$ are obtained by assembling the matrices found for the joints:

$$\mathcal{N}^0(q^0,q^1,\omega) = \begin{vmatrix} \mathcal{N}_1^0(q^0,q^1,\omega) \\ \mathcal{N}_2^0(q^0,q^1,\omega) \\ \vdots \\ \mathcal{N}_N^0(q^0,q^1,\omega) \end{vmatrix} \tag{22a}$$

$$\mathcal{N}^1(q^0,q^1,\omega) = \begin{vmatrix} \mathcal{N}_1^1(q^0,q^1,\omega) \\ \mathcal{N}_2^1(q^0,q^1,\omega) \\ \vdots \\ \mathcal{N}_N^1(q^0,q^1,\omega) \end{vmatrix} \tag{22b}$$

Under the single harmonic hypothesis, a limit cycle can occur in the controlled system if the state vector obeys Eq. (16). Furthermore, if the nonlinear feedback terms are expressed as in Eq. (17), then Eq. (14) yields the following relations to be satisfied by the parameters q^0, q^1, and ω:

$$(\Lambda + B_c G_1)q^0 = B_j \mathcal{N}^0(q^0,q^1,0)q^0 \tag{23a}$$

$$(-\omega^2 I + j\omega B_c G_2 + \Lambda + B_c G_1)q^1 = B_j \mathcal{N}^1(q^0,q^1,\omega)q^1 \tag{23b}$$

Introducing the following transfer function

$$G(s) = s^2 I + sB_c G_2 + \Lambda + B_c G_1 \tag{24}$$

system (23) can be rewritten as

$$[G(j0) - B_j \mathcal{N}^0(q^0,q^1,0)]q^0 = \mathbf{0} \tag{25a}$$

$$[G(j\omega) - B_j \mathcal{N}^1(q^0,q^1,\omega)]q^1 = \mathbf{0} \tag{25b}$$

along with the constraint

$$q^{1*}q^1 > 0 \tag{25c}$$

Equation (25a) is a system of n real algebraic equations. Equation (25b) is a system of n complex algebraic equations that can be developed as a system of $2n$ real algebraic equations; q^0 is an n-dimensional unknown real vector; q^1 is an n-dimensional unknown complex vector whose definition requires $2n$ real numbers. The phase of the first signal, however, can be chosen arbitrarily, and set, for example, to zero. The first element of q^1 will then be real, and only $2n-1$ parameters need to be found. The frequency ω being also unknown, the limit cycle conditions turn out to be a system of $3n$ real algebraic equations with $3n$ real unknowns.

V. Limit Cycle Stability

It is possible to determine stability analytically under the single harmonic hypothesis. In that case, only one class of perturbations, also called consistent perturbations, is considered, and this simplifies greatly the procedure.[4]

The approximate equation of the limit cycle in state space is one of an ellipse

$$q = q^0 + Re(q^1 \exp[j\omega(t - t_o)] \tag{26}$$

The ellipse is centered at q^0, and its principal axes are along the directions p^1 and p^2, defined as

$$p^1 = \alpha_1 Q_1 + \alpha_2 Q_2 \tag{27a}$$

$$p^2 = -\alpha_2 Q_1 + \alpha_1 Q_2 \tag{27b}$$

where

$$\alpha_1 = \frac{\|Q_1\|^2 - \|Q_2\|^2}{\|Q_1\|^2 + \|Q_2\|^2}, \qquad \alpha_2 = \frac{Q_1^T Q_2}{\|Q_1\|^2 + \|Q_2\|^2} \tag{28}$$

and

$$Q_1 = Re(q^1)$$

and

$$Q_2 = Im(q^1)$$

Perturbations δq^0, δq^1, and $\delta s = \delta\sigma + j\delta\omega$ yield new values for limit cycle parameters:

$$q_p^0 = q^0 + \delta q^0 \tag{29a}$$

$$q_p^1 = q^1 + \delta q^1 \tag{29b}$$

$$s_p = s + \delta\sigma + j\delta\omega, \qquad s = j\omega \tag{29c}$$

A perturbation is said to be consistent if the perturbed parameters satisfy Eqs. (25). That is, a consistent perturbation will be, to first order, in the plane of the ellipse that describes the limit cycle trajectory. As in bifurcation theory,[8] the system is believed to be stable in the subspace orthogonal to the limit cycle plane: hence, it is unnecessary to apply perturbations along this subspace.

Taking a first-order expansion of Eqs. (25) with respect to the limit cycle parameters, it is possible to relate $\delta\sigma$ to the rest of the perturbation parameters as

$$M\delta V = -P\delta\sigma \tag{30}$$

The perturbation vector is δV; $\delta V = [\delta q^0, Re(\delta q^1), Im(\delta q^1), \delta\omega]^T$. M is a $3n \times 3n$ matrix calculated by differentiating Eqs. (25) with respect to q^0, q^1, and ω. P is a $3n \times 1$ vector calculated by differentiating Eqs. (25) with respect to the complex variable s.

A stable limit cycle will attract the trajectories initiating in its neighborhood: if the initial conditions lie inside the ellipse, the corresponding $\delta\sigma$ must therefore be positive, and conversely, if the initial conditions lie outside the ellipse, $\delta\sigma$ must be negative for the limit cycle to be stable. The ellipse can be scaled to a circle of unit radius by an appropriate geometric transformation, that requires the knowledge of the center and the principal axes of the ellipse. Choosing an infinitesimal δV, it is possible to compute the corresponding perturbed initial point in state space using Eqs. (29), and to transform it using the geometric transformation that changed the ellipse into a circle. The resulting point is at a distance r from the center of the circle. The $\delta\sigma$ corresponding to δV is also computed using Eq. (30). The stability criterion for the limit cycle becomes then very simple: the scalar

$$\lambda = \delta\sigma(r - 1) \tag{31}$$

must be negative for the limit cycle to be stable.

VI. Numerical Resolution of the Limit Cycle Equations

One approach to solve the nonlinear algebraic system [Eqs. (25)] is to form the norm of the residual vector and to minimize it. A minimum at zero means that the equations are satisfied. A nonzero absolute minimum means that the limit cycle conditions cannot be met.

The residual vector is

$$\boldsymbol{R}(\boldsymbol{q}^0,\boldsymbol{q}^1,\omega)=\begin{bmatrix}[G(0)-B_j\mathcal{N}^0(\boldsymbol{q}^0,\boldsymbol{q}^1,0)]\boldsymbol{q}^0\\ Re\{[G(j\omega)-B_j\mathcal{N}^1(\boldsymbol{q}^0,\boldsymbol{q}^1,\omega)]\boldsymbol{q}^1\}\\ Im\{[G(j\omega)-B_j\mathcal{N}^1(\boldsymbol{q}^0,\boldsymbol{q}^1,\omega)]\boldsymbol{q}^1\}\end{bmatrix} \tag{32}$$

The residual function r will be

$$r(\boldsymbol{q}^0,\boldsymbol{q}^1,\omega)=\boldsymbol{R}^T(\boldsymbol{q}^0,\boldsymbol{q}^1,\omega)\boldsymbol{R}(\boldsymbol{q}^0,\boldsymbol{q}^1,\omega)/\boldsymbol{q}^{1*}\boldsymbol{q}^1 \tag{33}$$

The scaling by $\boldsymbol{q}^{1*}\boldsymbol{q}^1$ of the square of the norm of the residual vector prevents numerical searches from being trapped at a trivial equilibrium point, since the residual vector is zero when both $\boldsymbol{q}^0$ and $\boldsymbol{q}^1$ are zero.

Different numerical schemes were tried in Ref. 9. Computing the residual function is very long when the system considered needs a high dimensional state-space representation and has many distributed nonlinearities as well. In that case it was shown in Ref. 9 that quasi-Newton methods would be the fastest because of their high rate of convergence and their ability to generate both search directions and step sizes. The cost for estimating the optimal step size at each iteration is to estimate the Hessian of the residual function, which is done recursively using the gradient that is computed anyway. This extra computation is negligible when the computation of the residual is large. Nongradient methods suffer a much too low rate of convergence to make not computing the gradient worthwhile.

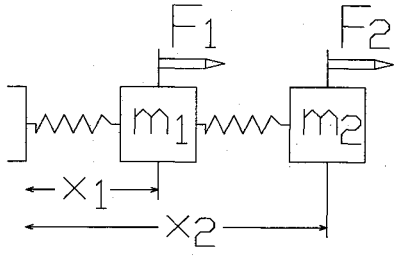

Fig. 3 Two-joint system.

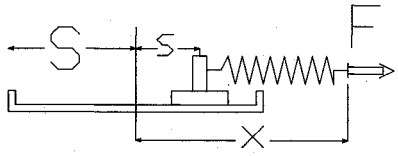

Fig. 4 Model of nonlinear joint.

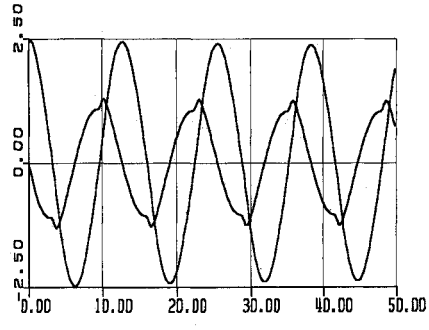

Fig. 5 Mass no. 1 displacement and rate of displacement.

Some properties of different numerical schemes are discussed in an example next.

VII. Limit Cycle and Stability Determination for a Simple Dynamical System

Let us take as an example a simple series of two masses held by nonlinear springs and attached to a fixed wall, as pictured in Fig. 3.

The masses are unitary. The full state is supposedly available for control purposes, and each mass can be independently driven by an actuator.

The following idealized joints (Fig. 4) approximate the behavior of the pinned joints retained in the COFS mast. They are constituted of a linear spring of unitary stiffness attached to a simple Coulomb friction element with threshold $Fc=0.1$. The sliding of the Coulomb element is limited to $\pm S$, where $S=0.5$. The joints are massless.

Such a joint can be modeled with two states, one giving the total deformation x, and one giving the sliding of the friction element s. The load-displacement law is simply

$$F=K(x-s), \qquad K=1 \tag{34}$$

and the dynamics of the joints are

$$\begin{cases}\dot{s}=\dot{x} & \text{if } |s|<S, \quad |F|=Fc, \quad \operatorname{sgn}(\dot{x})=\operatorname{sgn}(F)\\ \dot{s}=0 & \text{otherwise}\end{cases} \tag{35}$$

The load-displacement characteristics of the joints fall into hypothesis (1), since as x increases, s becomes negligible, and the load is asymptotically equal to $F=Kx$.

Use of the linear part of the joints allows one to build the linear part of the system. A multivariable PID feedback controller is implemented to modify the dynamics of the system. The integrators are used, first, to prevent the system from settling down in a steady state with constant biases, which occur otherwise, due to the loss of static accuracy resulting from the presence of the friction elements; second, to provide enough phase lag to make limit cycle possible.

The integral of the displacement, the displacement, and the rate of displacement of each mass form the state vector:

$$\boldsymbol{X}=\left[\int x_i\,dt,x_1,\dot{x}_1,\int x_2\,dt,x_2,\dot{x}_2\right]^T \tag{36}$$

The complete dynamical model becomes

$$\dot{\boldsymbol{X}}=\phi\boldsymbol{X}-\Gamma_c K\boldsymbol{X}+\Gamma_j\begin{bmatrix}F_1^{NL}\\ F_2^{NL}\end{bmatrix} \tag{37}$$

where

$$\phi=\begin{bmatrix}0&1&0&0&0&0\\0&0&1&0&0&0\\0&-2&0&0&1&0\\0&0&0&0&1&0\\0&0&0&0&0&1\\0&1&0&0&-1&0\end{bmatrix}$$

$$\Gamma_c=\begin{bmatrix}0&0&1&0&0&0\\0&0&0&0&0&1\end{bmatrix}^T$$

$$\Gamma_j=\begin{bmatrix}0&0&-1&0&0&0\\0&0&1&0&0&-1\end{bmatrix}^T$$

The F_i^{NL} are the remaining nonlinear parts of each joint. The displacements at the joints are gathered in a vector $\boldsymbol{d}$:

$$\boldsymbol{d}=\begin{vmatrix}d_1\\ d_2\end{vmatrix}=C\boldsymbol{X}, \qquad C=\begin{bmatrix}0&1&0&0&0&0\\0&-1&0&0&1&0\end{bmatrix} \tag{38}$$

The following gains were chosen using eigenstructure assignment:

$$K = \begin{bmatrix} 6.3156 & 4.4587 & 4.7650 & 5.4444 & 6.8613 & 1.1250 \\ 5.3056 & 6.8062 & 0.5750 & 6.4544 & 5.5138 & 5.2250 \end{bmatrix}$$

The poles of the closed-loop linear system are at $\lambda_1 = -4.0$, $\lambda_2 = -3.0$, $\lambda_{3-4} = -1.4 \pm j\,1.4$, $\lambda_{5-6} = -0.05 \pm j\,0.5$.

The damping ratios of the oscillatory modes are, respectively, 0.1 and 0.707, yielding only one closed-loop resonant mode. The displacements of the masses are forced by the controller to be opposite in phase along the resonant mode; $x_1 = -x_2$ when the system is oscillating along this mode.

Definitions similar to Eqs. (16) and (17) can be made, but in this particular case, there are fewer nonlinearities than modes, and the joint displacements d_1 and d_2 are the variables that will be preferred to derive the limit cycle conditions. The matrix function to use is the one that relates the nonlinear exciting forces to the joint displacement vector $\boldsymbol{d}$:

$$G = C(sI - \phi + \Gamma_c K)^{-1}\Gamma_j \tag{39}$$

Considering only the zero and first harmonics of $\boldsymbol{d}$ and $\boldsymbol{F}^{NL}$:

$$\boldsymbol{d} = \boldsymbol{B} + \boldsymbol{A}\exp(j\omega t) \tag{40a}$$

$$\boldsymbol{F}^{NL} = \boldsymbol{F}^0 + \boldsymbol{F}^1 \exp(j\omega t) \tag{40b}$$

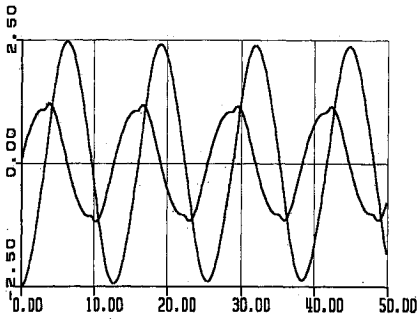

Fig. 6 Mass no. 2 displacement and rate of displacement.

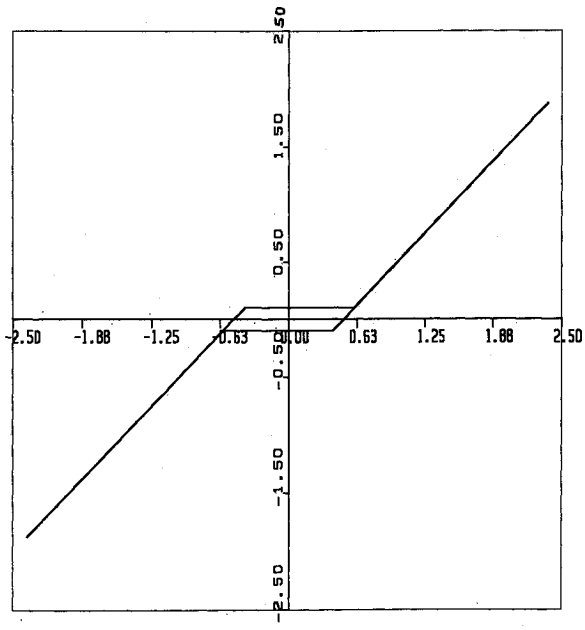

Fig. 7 Joint no. 1 load-displacement characteristics.

with $\boldsymbol{B} = [B_1, B_2]^T$ and $\boldsymbol{A} = [A_1, A_2 \exp(j\psi t)]^T$, the limit cycle conditions become

$$\boldsymbol{B} = G(0)\begin{bmatrix} n_B(A_1,B_1) & 0 \\ 0 & n_B(A_2,B_2) \end{bmatrix}\boldsymbol{B} \tag{41a}$$

$$\boldsymbol{A} = G(j\omega)\begin{bmatrix} n_A(A_1,B_1) & 0 \\ 0 & n_A(A_2,B_2) \end{bmatrix}\boldsymbol{A} \tag{41b}$$

G is the transfer function from the disturbance to the output, which is the sensitivity function of the linear system. Therefore, because of the integrators, $G(0)$, the steady-state sensitivity gain, is identically zero. There cannot, consequently, be any constant bias remaining in steady state, and $\boldsymbol{B}$ is zero. This result simplifies the problem, since only a sinusoidal input describing function (SIDF) has to be evaluated; $n_A(A,0)$ is the SIDF for the joint's load-displacement characteristic nonlinear remaining part (34):

$$F^{NL} = -Ks \tag{42}$$

Separating the real and the imaginary part as

$$n_A(A,0) = n_p(A,0) + jn_q(A,0)$$

the computation yields

$$\begin{cases} n_p(A,0) = 0 & \text{(43a)} \\ n_q(A,0) = 0 \qquad A < Fc & \text{(43b)} \end{cases}$$

$$\begin{cases} n_p(A,0) = \dfrac{1}{2}\left[-1 + f\left(\dfrac{2Fc - A}{A}\right)\right] & \text{(43c)} \\ n_q(A,0) = \dfrac{A^2 - (2Fc - A)^2}{\pi A^2} \qquad Fc < A < Fc + S & \text{(43d)} \end{cases}$$

$$\begin{cases} n_p(A,0) = \dfrac{1}{2}\left\{f\left[\dfrac{Fc - S}{A}\right] - f\left[\dfrac{Fc + S}{A}\right]\right\} & \text{(43e)} \\ n_q(A,0) = \dfrac{4FcS}{\pi A^2} \qquad A > Fc + S & \text{(43f)} \end{cases}$$

where

$$f(z)\begin{cases} = -1 & z < -1 \\ = \dfrac{2}{\pi}[\sin^{-1} z + \sqrt{1 - z^2}], & -1 < z < 1 \\ = +1, & z > 1 \end{cases} \tag{44}$$

The residual function becomes

$$R(A_1,A_2,\omega,\psi) = \left\| \begin{bmatrix} 1 & 0 \\ 0 & 1 \end{bmatrix} - G(j\omega)\begin{bmatrix} n_A(A_1,0) & 0 \\ 0 & n_A(A_2,0) \end{bmatrix} A \right\|^2 \Big/ A^*A \tag{45}$$

The conjugate gradient method as well as the Broyden-Fletcher-Goldfarb-Shanno (BFGS) quasi-Newton method were tried in Ref. 9 to search for possible limit cycles. Two limit cycles were found by both methods. The parameters of the limit cycles were found at

First limit cycle:

$$\begin{aligned} A_1 &= 2.3441 \\ A_2 &= 4.6675 \\ \psi &= 3.1351 \text{ rad} \\ \omega &= 0.4950 \text{ rad/s} \end{aligned} \tag{46}$$

corresponding to maximum mass displacements of $x_1 = 2.3441$ and $x_2 = 2.4234$.

Second limit cycle:

$$A_1 = 0.0698$$
$$A_2 = 0.1391$$
$$\psi = 3.1410 \text{ rad}$$
$$\omega = 0.4375 \text{ rad/s} \quad (47)$$

corresponding to maximum mass displacements of $x_1 = 0.0698$ and $x_2 = 0.0693$.

Only one limit cycle, with parameters corresponding to the first analytical conditions, was found by simulating the system. The amplitudes found for the joints' displacements after the system has reached steady state are, respectively, $A_1 = 2.3753$ and $A_2 = 4.7464$. The frequency is $\omega = 0.4893$ rad/s. The error between the simulated and the computed values is found to be here always less than 1.7%. It appears from this result, and from the shape of the signals plotted in Figs. 5 and 6, that the first harmonic hypothesis is satisfactorily met in this example. Figure 7 shows the hysteretic behavior of the load transmitted by joint 1. Figure 8 illustrates how the ellipse approximating the trajectory of the first mass in phase plane tries to match the real phase plane trajectory.

The state vector $\boldsymbol{X}$ has the following approximate expression when a limit cycle occurs:

$$\boldsymbol{X} = \boldsymbol{Q}_1 \cos(\omega t) + \boldsymbol{Q}_2 \sin(\omega t) \quad (48)$$

where

$$\boldsymbol{Q}_1 = [0, A_1, 0, A_2 \sin\psi/\omega, A_1 + A_2 \cos\psi, -A_2 \sin\psi\omega]^T \quad (49a)$$

$$\boldsymbol{Q}_2 = [A_1/\omega, 0, -A_1\omega(A_1 + A_2\cos\psi)/\omega, -A_2 \sin\psi, -(A_1 + A_2\cos\psi)\omega]^T \quad (49b)$$

It is necessary to compute the principal axes of the ellipse that approximates a limit cycle as a step to determine its stability. Plugging the set of parameters from Eq. (46) into Eqs. (49a) and (49b), and using Eqs. (27) and (28), yields the following principal axes for the first limit cycle:

$$\boldsymbol{p}_1 = [3.076 \times 10^{-2}, 2.3441, -7.54 \times 10^{-3}, 3.103 \times 10^{-2}, -2.3234, -7.60 \times 10^{-3}]^T$$

$$\boldsymbol{p}_2 = [4.7354, -1.523 \times 10^{-2}, -1.1604, -4.6937, -1.536 \times 10^{-2}, 1.1501]^T$$

The second step involves taking the derivatives of the limit cycle equations with respect to every parameter A_1, A_2, ω, and ψ. The corresponding matrix M and vector $\boldsymbol{P}$ are found to be

$$M = \begin{vmatrix} 0.9948 & -0.0013 & 0.0004 & -6.6431 \\ -0.0146 & -0.0072 & -1.5611 & 46.9348 \\ 0.0108 & -0.9974 & -0.0566 & 13.2108 \\ 0.0287 & 0.0209 & -7.7851 & -93.9046 \end{vmatrix}$$

$$\boldsymbol{P} = \begin{vmatrix} 46.9348 \\ 6.6431 \\ -93.9046 \\ -13.2108 \end{vmatrix}$$

The stability index λ can next be computed, and it is found in that case that $\lambda = -41.50\delta\sigma$, which means the limit cycle is *stable*. This result is confirmed by the simulation. Following the exact same steps for the second limit cycle, one can find the stability index to be $\lambda = +12.04\delta\sigma$, which indicates that the limit cycle is *unstable*. This explains the failure to simulate it.

The BFGS method was found superior to the conjugate gradient method.[9] For identical initial conditions, the former performed three times faster than the latter (Fig. 9). The quasi-Newton method was also found to be more robust, meaning that a change in the initial conditions rarely led the search to stall or diverge.

The choice of the initial point for the search process was found to be of great importance. Figure 10 displays the log of the residual function for the frequency ω between 0.01 and 10 rad/s, plotted in log scale, amplitudes $A_1 = A$ and $A_2 = 2^*A$, where A goes from 0 to 10, and for a phase $\psi = 180$ deg. This figure indicates that searches that start beyond the ridge appearing about the resonant frequency have little chance to converge. It was also shown in Ref. 9 that starting with the wrong phase information could be particularly detrimental for convergence, especially with the conjugate gradient method. Initial phase information can, however, be obtained by looking at the singular vector associated with the maximum singular value of the linear transfer function at the resonant frequency. Indeed, in the example just derived, the right singular vector associated with the maximum singular value at $\omega = 0.5$ rad/s corresponds to the following parameters: $A_2 = 1.9932\ A_1$ and $\psi = 3.1370$ rad. Those conditions are very close to the limit cycle conditions.

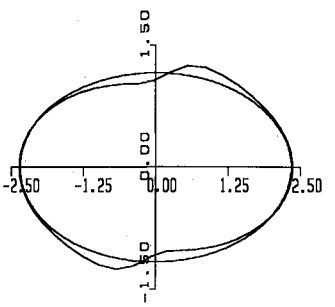

Fig. 8 Mass no. 1 trajectory in phase plane, simulated and approximated.

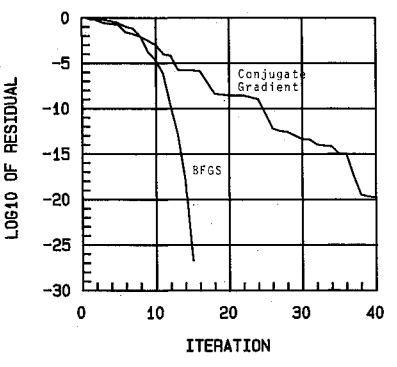

Fig. 9 Log of the residual during search with BFGS and conjugate gradient method.

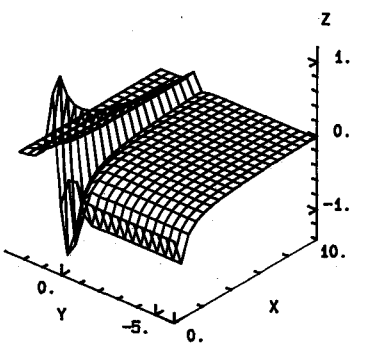

Fig. 10 Log of residual for $\omega = 0.01$ to 10 rad/s, $\psi = 180$ deg, $A_1 = 0$ to 10 and $A_2 = 2^*A_1$.

From the preceding remarks, it is believed that the initial conditions should lie along the singular vector associated with the linear transfer function maximum singular value at the resonant frequency. Also, the initial frequency should be below the resonant frequency, and the amplitudes should be small for the search not to diverge.

VIII. Conclusion

It is possible to model an actively controlled truss structure with nonlinear joints as a linear system with nonlinear feedback by separating the joint load-displacement characteristics into a linear part, which prevails at large displacements, and a nonlinear part. Replacing the joints by their linear parts, a standard modal decomposition can be performed, yielding a reduced-order linear model. Linear control laws can be easily included in the linear part of the system; nonlinear control laws can be implemented, but they must be fed back with the nonlinear part of the joint characteristics that were overlooked to develop a linear model.

Limit cycle analysis is straightforward when such a modeling is done. High-frequency resonant peaks are supposedly filtered out because of the feedback control loop. The signals can thus be approximated only to their first harmonic with reasonable accuracy. The use of DIDF allows a simple treatment of the nonlinear effects. The conditions for the existence of a limit cycle turn out to be in that case a system of nonlinear algebraic equations. This system of equations can be solved numerically using, for example, quasi-Newton methods, which have proven to be very successful for that problem. For reduced-order systems, the method is very successful in giving an accurate prediction of the limit cycle parameters, even with consistently important nonlinearities.

The procedure, however, suffers one important drawback in that the computations grow rapidly as the number of distributed nonlinearities increases. The residual function requires that the nonlinear effects of every nonlinearity on every mode be computed. As many as 1000 joints are used in structures like the COFS mast; in that case, the method cannot be implemented without further simplifications, and the condensing of the number of distributed nonlinearities retained in the model.

Acknowledgment

This work was sponsored by NASA Langley Research Center under Grant NAG-1-126.

References

[1]Minorsky, N., *Theory of Nonlinear Control Systems*, McGraw-Hill, New York, 1969.

[2]Atherton, D. P., *Stability of Nonlinear Systems*, Research Study Press, 1981.

[3]Cook, P. A., *Nonlinear Dynamical Systems*, Prentice-Hall International, 1986.

[4]Aderibigbe, A. A., "Methods for Predicting Limit Cycles in Multivariable Nonlinear Dynamic Systems," Ph.D. Thesis, Dept. of Mechanical Engineering, Massachusetts Inst. of Technology, Cambridge, MA, 1986.

[5]Nayfeh, A. H. and Mook, D. T., *Nonlinear Oscillations*, Wiley-Interscience, New York, 1979, Chap. 7.

[6]Meirovitch, L., *Computational Methods in Structural Dynamics*, Sithoff-Noordhoff, 1980.

[7]Gelb, A. and Vander Velde, W. E., *Multiple-Input Describing Functions and Nonlinear System Design*, McGraw-Hill, New York, 1968.

[8]Guckenheimer, J. and Holmes, P., *Nonlinear Oscillations, Dynamical Systems, and Bifurcation of Vector Fields*, Springer-Verlag, New York, 1983.

[9]Mercadal, M., "Joint Nonlinearity Effects in the Design of a Flexible Truss Structure Control System," S.M. Thesis, Dept. of Aeronautics and Astronautics, Massachusetts Inst. of Technology, Cambridge, MA, 1986.